Pergamon

www.neuroscience-ibro.com

PII: S0306-4522(02)00237-3

Neuroscience Vol. 113, No. 4, pp. 809–823, 2002

0306-4522/02 $22.00+0.00

IMMUNOREACTIVE LOCALISATION OF $P2Y_1$ RECEPTORS WITHIN THE RAT AND HUMAN NODOSE GANGLIA AND RAT BRAINSTEM: COMPARISON WITH [α^{33}P]DEOXYADENOSINE 5′-TRIPHOSPHATE AUTORADIOGRAPHY

A. Y. FONG,[a] E. V. KRSTEW,[a] J. BARDEN[b] and A. J. LAWRENCE[a]*

[a]Department of Pharmacology, P.O. Box 13E, Monash University, Wellington Road, Clayton, Vic. 3800, Australia

[b]Institute of Biomedical Research, University of Sydney, Sydney, NSW 2006, Australia

Abstract—The present study employed standard peroxidase immunohistochemistry to map the distribution of $P2Y_1$ receptors in the rat brainstem and nodose ganglia and characterised the binding profile of [α^{33}P]dATP. Binding of [α^{33}P]dATP was fully displaceable by adenosine 5′-triphosphate (ATP), and was found on both human and rat nodose ganglia, and throughout the rat brainstem, including the nucleus tractus solitarius and ventrolateral medulla. [α^{33}P]dATP binding in the human nodose ganglia was significantly displaced by both 2-methylthio ATP and α,β-methylene ATP, but not by uridine 5′-triphosphate, pyridoxalphosphate-6-azophenyl-2′,4′-disulfonic acid, 8,8′-(carbonylbis(imino-4,1-phenylenecarbonylimino-4,1-phenylenecarbonylimino))bis(1,3,5-naphtalenetrisulfonic) acid (NF279) or *N*-ethylcarboxamidoadenosine. [α^{33}P]dATP binding in the rat nodose ganglia and brainstem was significantly displaced by only 2-methylthio ATP, suggesting that [α^{33}P]dATP is binding to P2Y receptors in the rat. Binding of [α^{33}P]dATP was also significantly displaced by α,β-methylene adenosine 5′-diphosphate, suggesting a component of the binding is to endogenous ecto-5′-nucleotidase, however, almost all binding could be displaced by a combination of receptor agonists (2-methylthio ATP, uridine 5′-triphosphate and α,β-methylene ATP), suggesting preferential binding to receptors. Immunoreactivity to $P2Y_1$ receptor ($P2Y_1$-IR) exhibited similar distribution patterns to [α^{33}P]dATP binding, with a clear topographic profile. Particularly dense $P2Y_1$-IR labeling was evident in cells and fibres of the dorsal vagal complex. Immunolabeling was also present in the dorsal motor nucleus of the vagus and nucleus ambiguus, indicating the possibility of $P2Y_1$ receptors on vagal efferents. Unilateral vagal ligation was also performed to examine the transport of $P2Y_1$ receptor, using both immunohistochemistry and [α^{33}P]dATP autoradiography. Accumulations of both $P2Y_1$-IR and [α^{33}P]dATP binding were apparent adjacent to both ligatures, suggesting bi-directional transport of $P2Y_1$ receptors along the rat vagus nerve. This current study represents the first description of $P2Y_1$ receptor distribution within the rodent brainstem and nodose ganglion and also characterises [α^{33}P]dATP binding to P2Y receptors. © 2002 IBRO. Published by Elsevier Science Ltd. All rights reserved.

Key words: P2-purinoceptors, Adenosine 5′-triphosphate, autonomic regulation, autoradiography, immunohistochemistry.

The purine nucleotide, adenosine 5′-triphosphate (ATP) is now widely accepted as a fast excitatory neurotransmitter, capable of acting both centrally (Edwards et al., 1992) and peripherally (Evans et al., 1992). There is increasing evidence to suggest the importance of purinergic neurotransmission as an integral part of central autonomic control. Studies have shown that ATP appears to act in a neurotransmitter-like manner in a number of nuclei associated with autonomic control, such as the nucleus tractus solitarius (NTS) (Barraco et al., 1996; Ergene et al., 1994; Scislo et al., 1998; Scislo and O'Leary, 2000), caudal and rostral ventrolateral medulla (CVLM/RVLM) (Horiuchi et al., 1999; Ralevic et al., 1999; Sun et al., 1992; Thomas and Spyer, 2000), and the pontine locus coeruleus (LC) (Nieber et al., 1997; Shen and North, 1993). In addition, ATP apparently

*Corresponding author. Tel.: +613-9905-4855; fax: +613-9905-5851. *E-mail address:* andrew.lawrence@med.monash.edu.au (A. J. Lawrence).

Abbreviations: α,βMeADP, α,β-methylene adenosine 5′-diphosphate; α,βMeATP, α,β-methylene adenosine 5′-triphosphate; ANOVA, analysis of variance; AP, area postrema; ATP, adenosine 5′-triphosphate; cNTS, commissural nucleus tractus solitarius; Cu, cuneate nucleus; CVLM, caudal ventrolateral medulla; DMX, dorsal motor nucleus of the vagus; DPM, disintegrations per minute; DVC, dorsal vagal complex; ECu, external cuneate nucleus; EDTA, ethylenediaminetetra-acetic acid disodium salt; Gr, gracile nucleus; HRP, horseradish peroxidase; IOC, inferior olivary complex; IR, immunoreactivity; LRt, lateral reticular nucleus; 2MeSATP, 2-methylthio adenosine 5′-triphosphate; mNTS, medial nucleus tractus solitarius; NECA, *N*-ethylcarboxamidoadenosine; NF279, 8,8′-(carbonylbis(imino-4,1-phenylenecarbonylimino-4,1-phenylenecarbonylimino))bis(1,3,5-naphthalenetrisulfonic) acid; NHS, normal horse serum; NRS, normal rabbit serum; NTS, nucleus tractus solitarius; PBS, phosphate-buffered saline; PPADS, pyridoxalphosphate-6-azophenyl-2′,4′-disulfonic acid; RVLM, rostral ventrolateral medulla; SDS, sodium dodecyl sulphate; Sp5, spinal trigeminal nucleus; spNTS, subpostremal nucleus tractus solitarius; UTP, uridine 5′-triphosphate.

acts as a cotransmitter with noradrenaline in the sympathetic nervous system (Burnstock, 1995; Meldrum and Burnstock, 1985).

The actions of ATP are mediated via cell surface receptors, termed P2-purinoceptors (Ralevic and Burnstock, 1998). The P2-purinoceptors are subdivided into two major classes, based on their structural and pharmacological profiles, P2X and P2Y. P2X receptors contain two transmembrane domains and are ligand-gated ion channels, which cause membrane depolarisation and a voltage-dependent Ca^{2+} influx upon activation (Mateo et al., 1998). P2Y-purinoceptors are heptahelical, G protein-coupled receptors, mediating signal transduction via the induction of inositol triphosphate (IP3), leading to intracellular Ca^{2+} release (Strobaek et al., 1996), though some evidence also indicates linkage of P2Y receptors to adenylate cyclase (Boyer et al., 2000; Webb et al., 1996) and N-type calcium channels (Filippov et al., 2000). Thus, P2Y receptors appear to have a modulatory role, rather than directly mediating purinergic transmission.

To date, seven mammalian P2Y receptors have been cloned and shown to be activated by extracellular nucleotides; namely $P2Y_1$, $P2Y_2$, $P2Y_4$, $P2Y_6$, $P2Y_{11}$, and the more recent $P2Y_{12}$ (Hollopeter et al., 2001; Zhang et al., 2001) and $P2Y_{13}$ (Communi et al., 2001) receptors, although not all have been cloned from the rat (for a review, von Kügelgen and Wetter, 2000). However, extensive pharmacological and physiological studies on P2Y receptor-mediated events have been impeded due to the lack of readily available subtype selective ligands, though a number of tools are becoming available (Boyer et al., 1996; Kim et al., 2000; Schachter and Harden, 1997; Vigne et al., 1999, 2000; Zundorf et al., 2001). While the expression of P2Y receptor subtypes have been found within a number of tissue types, including the brain (Simon et al., 1997; Webb et al., 1998), the localisation and distribution of P2Y receptor subtypes within the brain remains largely unknown. While two recent studies have described immunoreactivity to $P2Y_1$ receptor ($P2Y_1$-IR) in rodent (Moran-Jimenez and Matute, 2000) and human (Moore et al., 2000) forebrain, there are no such studies in brainstem. The radioligand [^{35}S]dATPαS has been employed to label P2Y receptors (Simon et al., 1997; Webb et al., 1998), although selectivity for $P2Y_1$ receptors has been challenged (Schachter and Harden, 1997). Thus, dATP has agonist activity at $P2Y_1$, $P2Y_2$ and $P2Y_{11}$ receptors (Schachter and Harden, 1997; Communi et al., 1999), while dATPαS may also have agonist actions at some P2X receptors (Pubill et al., 2001). Furthermore, it remains to be established whether dATP has agonist activity at $P2Y_{12}$ and $P2Y_{13}$ receptors. Due to the lack of selective radioligands, the present study aims to (1) characterise the binding of [α^{33}P]dATP to P2 receptors on human and rat nodose ganglia and rat brainstem, and (2) employ the technique of immunohistochemistry, utilising a polyclonal antibody raised against the $P2Y_1$ receptor, to map the distribution of $P2Y_1$ receptors within the rat medulla oblongata and nodose ganglion. In addition, possible axonal transport of this protein along the rat vagus nerve will be examined using both autoradiography and immunohistochemistry.

EXPERIMENTAL PROCEDURES

All experiments were performed in accordance with the Prevention of Cruelty to Animals Act 1986 and under the guidelines of the National Health and Medical Research Council (NH&MRC) Code of Practice for the Care and Use of Animals for Experimental Purposes in Australia. Efforts were made to minimise animal suffering and the number of animals used.

Animals

Adult, male Wistar–Kyoto rats used in this study were obtained from the Biological Research Laboratory, Austin Hospital, Melbourne, Australia, group housed at a constant temperature of 22°C, with a relative humidity of 50–60%, under a controlled 12 h light–dark cycle. The rats were given access to food (standard laboratory chow) and water *ad libitum*.

Surgical procedures

Nine male, Wistar–Kyoto rats (310–380 g) were anaesthetised with ketamine/xylazine (60/7.8 mg/kg, i.p.), before a standard unilateral vagal ligation was performed as previously described (Fong et al., 2000; Lawrence et al., 1995). Of the nine rats, four were used for the autoradiographic study and five were used for the immunohistochemical study. In short, the left vagus nerve, distal to the nodose ganglion, was exposed and two ligatures (3/0 silk, Davis and Geck, Baulkham Hills, NSW, Australia), ~5 mm apart were secured around the vagus nerve. The right vagus nerve was exposed and served as sham control. The wounds were sutured, infiltrated with lidocaine (1% w/v, Delta West) and dusted with Cicatrin® antibiotic powder (Wellcome). The rats were housed individually during the 2-day recovery period and allowed food and water *ad libitum*.

Tissue preparation

Autoradiography. Human nodose ganglia. Inferior vagal ganglia were obtained from cadavers at the Victorian Institute of Forensic Pathology (VIFP). Ethical permission was granted by the Ethics and Integrity in Research Committees of both Monash University and the Victorian Institute of Forensic Pathology. Donors ($n = 4$) were males between the age of 18 and 76 years old, with no previous record of neurological disease. In all cases, the time between death and autopsy was < 48 h. Immediately following dissection, the ganglia were frozen over liquid nitrogen, transported in dry ice for storage at −80°C until use. Longitudinal sections (14 μm) were cut on a cryostat (Cryocut 1800, Reichert-Jung) at −18°C, thaw-mounted onto gelatin/chrome-alum subbed glass microscope slides and stored at −80°C until use.

Rat nodose ganglia and brainstem. At the end of the recovery period following unilateral vagal ligation, the rats were re-anaesthetised with ketamine/xylazine (60/7.8 mg/kg, i.p.), the left and right nodose ganglia and distal vagus nerves were excised, the ligatures removed and the tissue frozen in embedding medium (OCT tissue embedding compound, Miles Diagnostics) over supercooled isopentane. The rats were decapitated, brainstems removed and frozen over liquid nitrogen. Longitudinal sections of the nodose ganglia/vagus nerve (10 μm) and coronal sections of brainstem (14 μm) were cut on a cryostat, thaw-mounted onto gelatin/chrome-alum subbed glass microscope slides and stored at −80°C until use.

Immunohistochemistry. Rats having undergone unilateral vagal ligation ($n = 5$) and unoperated rats ($n = 6$) were anaesthetised with sodium pentobarbitone (60 mg/kg, i.p.) and transcardially perfused with 100 ml phosphate-buffered saline (0.1 M PBS, pH 7.4) at room temperature followed by 400 ml of 4% paraformaldehyde (w/v) in 0.1 M PBS (pH 7.4). The brains and/or nodose ganglia were removed, stored and cryoprotected in fixative containing 10% sucrose overnight at 4°C. The following morning, the nodose ganglia and adjacent vagus nerve were frozen in embedding medium over supercooled isopentane, and longitudinal sections (10 μm) were collected on a cryostat

and thaw-mounted onto gelatin/chrome-alum subbed glass microscope slides. Coronal sections (50 μm) were cut on a freezing microtome (Leitz) throughout the extent of the brainstem, placed in tissue culture plates containing 0.1 M PBS and processed for immunohistochemical detection of P2Y$_1$ receptors.

[α^{33}P]dATP autoradiography

The protocol for [α^{33}P]dATP autoradiography was adapted from a previously published protocol utilising [^{35}S]dATPαS (Simon et al., 1997). The slide-mounted sections were removed from −80°C and allowed to return to room temperature, before incubation for 30 min in Tris–HCl (50 mM) buffer with EDTA (1 mM), pH 7.4, at room temperature. The sections were then incubated for 30 min in the presence of 0.7 nM [α^{33}P]dATP (NEN DuPont, specific activity 3000 Ci/mmol), in Tris–HCl (50 mM) with EDTA (1 mM, pH 7.4) at room temperature. Non-specific binding was examined on adjacent sections in the presence of ATP (1 mM, Sigma Chemical Co.). Displacement of binding by various ligands was examined on adjacent sections of the human and rat nodose ganglia and rat brainstem in the presence of *N*-ethylcarboxamidoadenosine (NECA, 10 μM, Research Biochemicals Incorporated), pyridoxalphosphate-6-azophenyl-2′4′-disulfonic acid (PPADS, 100 μM, Tocris-Cookson), 8,8′-(carbonylbis(imino-4,1-phenylenecarbonylimino-4,1-phenylenecarbonylimino))bis(1,3,5-naphtalenetrisulfonic) acid (NF279, 1 μM, Tocris-Cookson), α,β-methylene ATP (α,βMeATP, 100 μM, Sigma Chemical Co.), uridine 5′-triphosphate (UTP, 100 μM, Sigma Chemical Co.) and 2-methylthio ATP (2MeSATP, 1 μM, Tocris-Cookson). In addition, displacement of binding by the ecto-5′-nucleotidase inhibitor, α,β-methylene adenosine 5′-diphosphate (α,βMeADP, 100 μM, Sigma Chemical Co.) and combinations of agonists (α,βMeATP+UTP+2MeSATP) in the presence and absence of α,βMeADP were also examined in the rat nodose ganglia and brainstem sections. After incubation, the sections were washed briefly (2×30 s) in ice-cold Tris–HCl buffer (50 mM, pH 7.4) before rinsing in ice-cold deionised water. The sections were then dried in a cool stream of air, desiccated overnight and apposed to autoradiographic film (Kodak X-omat) for 4–27 h, in the presence of ^{14}C standard microscales (American Radiolabeled Chemicals Inc., USA).

P2Y$_1$ receptor immunohistochemistry

Antibody production. The P2Y$_1$ antibody employed in the present study was raised in sheep using a standard protocol (see Yao et al., 2000). In brief, the epitope peptide was chosen as extracellular residues from the first (N-terminal) extracellular segment encompassing the segment 36–51 of the rat P2Y$_1$ sequence, VSSSFRCALIKTGFQFY but with the C42 replaced with S42 and a C-terminal Cys added for crosslinking to a 6 kDa diphtheria toxin domain via the maleimidocaproyl-*N*-hydroxysuccinimide (MCS) crosslinker (10:1 ratio of epitope:diphtheria toxin). The corresponding human epitope, VSSSFKCALTKTGFQFY, varies by only two residues. The peptide antigen conjugates were suspended in water at 5 mg/ml and aliquots emulsified by mixing with complete Freund's adjuvant. Emulsion volumes of 1 ml, containing 2 mg of peptide, were injected i.m. with second, third, forth and fifth immunisations following 2-week intervals using incomplete Freund's adjuvant. Final bleeds via venepuncture were obtained at 12 weeks, after it was established that adequate antibody titres had been obtained. The blood was incubated at 37°C for 30 min and stored at 4°C for 15 h after the serum was collected following centrifugation and stored at −20°C in small aliquots. Sera were tested with an enzyme-linked immunosorbent assay (ELISA) for antibodies specific to the peptide.

Western blots. Tissue samples were prepared from fresh rat midbrains. These were homogenised using a Polytron homogeniser (model PT1200) run at maximum speed for 10×30 s bursts in six volumes of PBS/0.5% Triton buffer, including protease inhibitors (Complete Protease Inhibitor Cocktail Tablets, Boehringer Mannheim). Standard sodium dodecyl sulphate–polyacrylamide gel electrophoresis (SDS–PAGE) procedures were undertaken using a NOVEX X-cell II mini system running 10–20% gradient gels. Tissue loadings were 0.2 mg/ml in PBS containing protease inhibitors. 0.2 ml of the homogenate was diluted with 0.05 ml of six times SDS-reducing buffer (sample) and 0.015 ml of this loaded onto the gels. Protein was transferred from the gels to nitrocellulose membranes (Amersham) using a NOVEX X Cell II Blot Module and transfer buffer (2.9 g glycine, 5.8 g Tris, 0.37 g SDS, 20% methanol in 1 l). Membranes were blocked with PBS/2% skim milk powder for 12 h and rinsed (3×15 min) with PBS/0.1% Tween/2% skim milk powder. Sheep P2Y$_1$ serum, with or without pre-absorption of the conjugated peptide epitope (10 μM), and pre-immune serum were used at 1:200 concentration and anti-sheep horseradish peroxidase (HRP) was used at a 1:5000 concentration. Primary antibodies were incubated for 1 h while the secondary antibody was incubated for 30 min. Detection of antibody bands was achieved using the ECL/Hyperfilm system (Amersham).

Pre-absorption controls. Sections of rat tail artery (30 μm) or midbrain (30 μm) were washed with 0.1% dimethyl sulfoxide (DMSO) in phosphate-buffered normal horse serum (100 ml PBS, 2 ml normal horse serum (NHS), 0.1 ml Triton X-100, 1 g bovine serum albumin (BSA)) for 30 min to permeabilise cellular membranes. Preparations were washed in PBS (0.1 M, 30 min with several changes of solution) and blocked with 20% NHS for 1 h. This was followed by incubation with 1:200 of the sheep anti-P2Y$_1$ antisera. Incubation with primary antibody was carried out for 12 h at room temperature in a humidified container either in the absence of epitope or after pre-incubation for 12 h with the conjugated peptide epitope (10 μM). Slides were washed for 30 min, again with several changes of PBS and then incubated in anti-sheep Cy3 (Jackson Immunoresearch, USA) for 1 h. The slides were washed for 40 min (with several changes of PBS), coverslipped using gelatin glycerol mountant and sealed. All sections were viewed on a Leica TCS NT laser confocal microscope system, as previously described (Yao et al., 2000).

Peroxidase immunohistochemistry. The immunocytochemical procedure used in the present study was adapted from those described previously (Lawrence et al., 1998; Yao et al., 2000), using crude serum. Free-floating or slide-mounted sections were incubated for 15 min in a pre-block medium comprising of 10% normal rabbit serum (NRS) and Triton X-100 (0.3%, Ajax) in PBS (0.1 M, pH 7.4) prior to subsequent rinses in PBS (3×5 min). Following the pre-block, the sections were incubated in sheep anti-P2Y$_1$ serum (1:3000 dilution) in PBS (0.1 M) containing NRS (1%) and Triton X-100 (0.3%) for 24–36 h at 4°C. Following the primary antibody incubation, the sections were rinsed in PBS (3×15 min), then incubated with rabbit anti-sheep biotinylated immunoglobulin (IgG) (1:500, Vector Laboratories) with NRS (1%) and Triton X-100 (0.3%) in PBS (0.1 M) for 1 h at room temperature. After further rinsing in PBS (3×15 min) sections were incubated for 1 h with streptavidin-conjugated HRP (1:200, Silenus) in PBS (0.1 M) with NRS (1%) and Triton X-100 (0.3%). Subsequent to further washes (3×15 min), the sections were exposed to cobalt-nickel enhanced diaminobenzidine (DAB; Pierce) for 15–20 min. The colour reaction was terminated by dilution with PBS. Control experiments included either incubation of the sections in the absence of primary antisera or in the absence of the secondary antisera. Sections were then mounted onto glass microscope slides with 0.5% gelatin (w/v) and allowed to air dry. Once dried, the sections were dehydrated in serial ethanol (70%, 90%, 3×100%), cleared and coverslipped.

A subset of sections from unilaterally ligated rat vagus nerves underwent P2X$_2$ receptor immunohistochemistry as a positive control for vagal transport. The protocol for anti-P2X$_2$ receptor immunohistochemistry was performed as described previously (Yao et al., 2000).

Data analysis and photomicroscopy

Autoradiography. Subsequent to autoradiogram development, densitometric analysis was performed using the Scion Image Analysis System (PC version, National Institute of Health (NIH) Image) by comparison of optical densities of autoradiograms with standard microscales under constant illumination. Results were expressed as disintegrations per minute (DPM)/mm^2. Brain regions were identified with reference to a stereotaxic atlas (Paxinos and Watson, 1986). Subsequent to densitometric analysis, displacement data were expressed as % total binding.

Immunohistochemistry. Sections processed for immunohistochemistry were examined using an Olympus BH-2 microscope. Photographs of the sections were taken with a Nikon-camera using Ilford FP4+ film. A semi-quantitative analysis of the labeling observed was made by counting the number of immunopositive cells within the defined borders of the respective nuclei, with reference to a stereotaxic atlas of the rat brain (Paxinos and Watson, 1986). The number of labelled cell bodies throughout the brainstem were scored in the following manner: 0 cells (−), <10 cells (+), 10–19 cells (++), 20–49 cells (+++), >50 cells (++++). For descriptive purposes the terms absent (−), detectable (+), low (++), moderate (+++) and high (++++) will be used in the text.

Statistical analysis. One-way analysis of variance (ANOVA) followed by Bonferroni's correction for multiple comparisons was performed on displacement studies in the human nodose ganglia, rat nodose ganglia and rat brainstem. Raw data were used for these above statistical tests. One-way repeated measures ANOVA, followed by Bonferroni's *t*-test was used for comparison of total binding between different subregions of the NTS. In all cases, $P < 0.05$ was considered significant.

RESULTS

[α^{33}P]dATP autoradiography

Human inferior vagal ganglion. Punctate binding of [α^{33}P]dATP was observed over sections of human inferior vagal ganglia (Fig. 1A). [α^{33}P]dATP binding (188 ± 16 DPM/mm^2) was fully displaced by ATP (1 mM). There was no significant displacement of binding by NECA, PPADS, NF279 or UTP (Fig. 1B); however, α,βMeATP (Fig. 1C) and 2MeSATP (Fig. 1D) could partially displace [α^{33}P]dATP binding (Table 1).

Rat nodose ganglia. Binding of [α^{33}P]dATP was present on the rat nodose ganglia and the vagus nerve (Fig. 2A). Binding of [α^{33}P]dATP (185 ± 38 DPM/mm^2) was fully displaced by ATP (1 mM) similar to the human inferior vagal ganglion. In contrast to binding in the human inferior vagal ganglia, α,βMeATP (Fig. 2B) failed to displace [α^{33}P]dATP binding, while the inclusion of 2MeSATP (Fig. 2C) or α,βMeADP significantly inhibited binding of [α^{33}P]dATP. Inclusion of NECA, PPADS or NF279 in the incubation tended to potentiate the level of [α^{33}P]dATP binding, although this increase was not significantly different to total binding (Table 1). Displacement by the combination of agonists (UTP, α,βMeATP and 2MeSATP) with or without α,βMeADP significantly inhibited binding of [α^{33}P]dATP, such that the remaining binding was almost undetectable (Table 1).

Rat unilateral vagal ligation. Following unilateral vagal ligation, [α^{33}P]dATP binding was apparent adjacent to both the proximal and distal ligatures (Fig. 2D). Displacement by 2MeSATP (Fig. 2F) and α,βMeADP (Fig. 2E) both significantly reduced [α^{33}P]dATP binding by ~76.5% and 60%, compared to total binding, respectively (Table 1). Displacement by combinations of agonists (UTP, α,βMeATP and 2MeSATP) with or without α,βMeADP reduced binding adjacent to ligature sites to undetectable levels (Table 1).

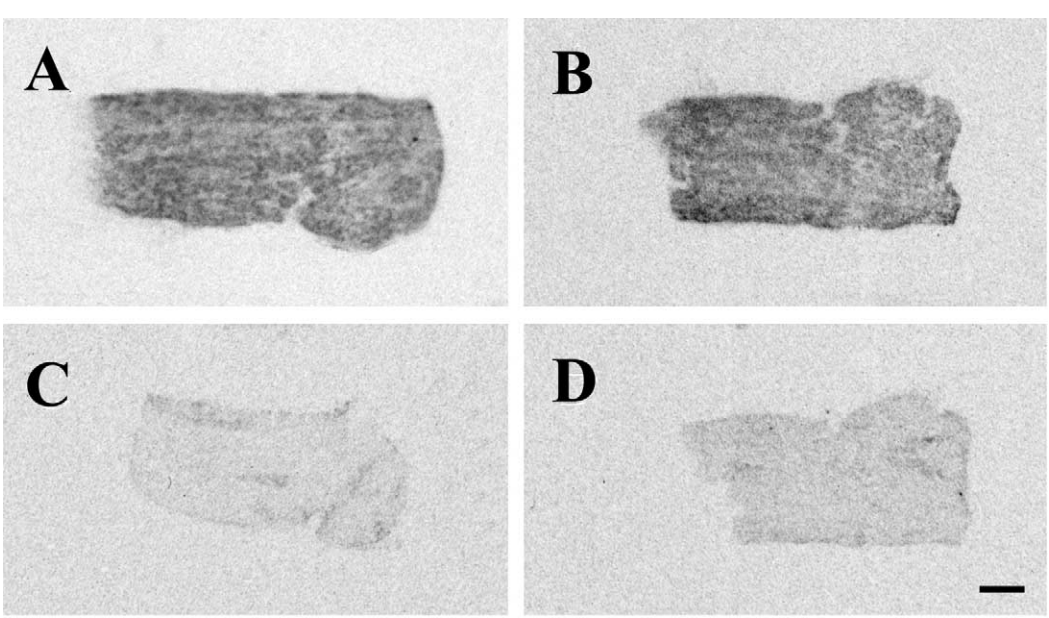

Fig. 1. Representative autoradiograms of [α^{33}P]dATP binding in the human inferior vagal ganglion. (A) Total binding of [α^{33}P]dATP, showing the punctate distribution of binding throughout the entire section. (B) Binding in the presence of UTP (100 μM) did not significantly affect the binding of [α^{33}P]dATP. (C, D) [α^{33}P]dATP binding in the presence of both α,βMeATP (100 μM, C) and 2MeSATP (1 μM) was significantly inhibited. Scale bar = 2 mm.

Table 1. Percentage of total [α^{33}P]dATP binding in human and rat nodose ganglia, and the effect of unilateral vagal ligation, in the presence of various displacers

Displacers	Conc. (M)	Human nodose ganglia	Rat nodose ganglia	Rat vagal ligation accumulation
NECA	10 μM	86 ± 5	137 ± 10	154 ± 14
PPADS	100 μM	86 ± 3	123 ± 13	162 ± 32
NF279	1 μM	101 ± 6	125 ± 13	177 ± 46
UTP	100 μM	89 ± 9	70 ± 17	67 ± 21
α,βMeATP	100 μM	39 ± 4*	57 ± 6	76 ± 12
2MeSATP	1 μM	42 ± 5*	22 ± 4*	24 ± 4*
α,βMeADP	100 μM		33 ± 4*	40 ± 9*
UTP	100 μM		6 ± 1*	1 ± 0.1*
α,βMeATP	100 μM			
2MeSATP	1 μM			
UTP	100 μM		6 ± 1*	1 ± 0.1*
α,βMeATP	100 μM			
2MeSATP	1 μM			
α,βMeADP	100 μM			

Data represent the mean of observations made over four sections per displacer in $n = 4$ subjects for human nodose ganglia. Data for rat nodose ganglia and rat vagal ligation accumulation represent mean of observations made over a minimum of four sections per rat.

*Comparison of % binding in the presence of various displacers versus total binding within species. $P < 0.05$, one-way ANOVA, post hoc Bonferroni's *t*-test.

Dorsal vagal complex (DVC). Binding of [α^{33}P]dATP was apparent in the DVC, throughout the rostro-caudal extent of the NTS and area postrema (AP) (Fig. 3A–C). Total binding, as determined by densitometric analysis, expressed as DPM/mm^2 is presented in Table 2. Subpostremal NTS (spNTS) was found to have significantly lower [α^{33}P]dATP binding compared to commissural NTS (cNTS). Binding of [α^{33}P]dATP was completely displaced by ATP (1 mM). A trend towards potentiation of [α^{33}P]dATP binding was observed in the presence of NECA (19.5–61.1%), PPADS (9.5–30.2%) and NF279 (up to 15.8%), though these differences were not significant (Table 2). Incubation with α,βMeATP (Fig. 3D) or UTP did not significantly inhibit binding of [α^{33}P]dATP. Significant inhibition of [α^{33}P]dATP binding was observed in the presence of 2MeSATP (Fig. 3F), α,βMeADP (Fig. 3E), and in the presence of a combination of agonists (UTP+α,β MeATP+2MeSATP) with or without α,βMeADP (Table 2). A combination of all three agonists (UTP, α,βMeATP and 2MeSATP) in the presence or absence of α,βMeADP resulted in almost complete inhibition of [α^{33}P]dATP binding (Table 2).

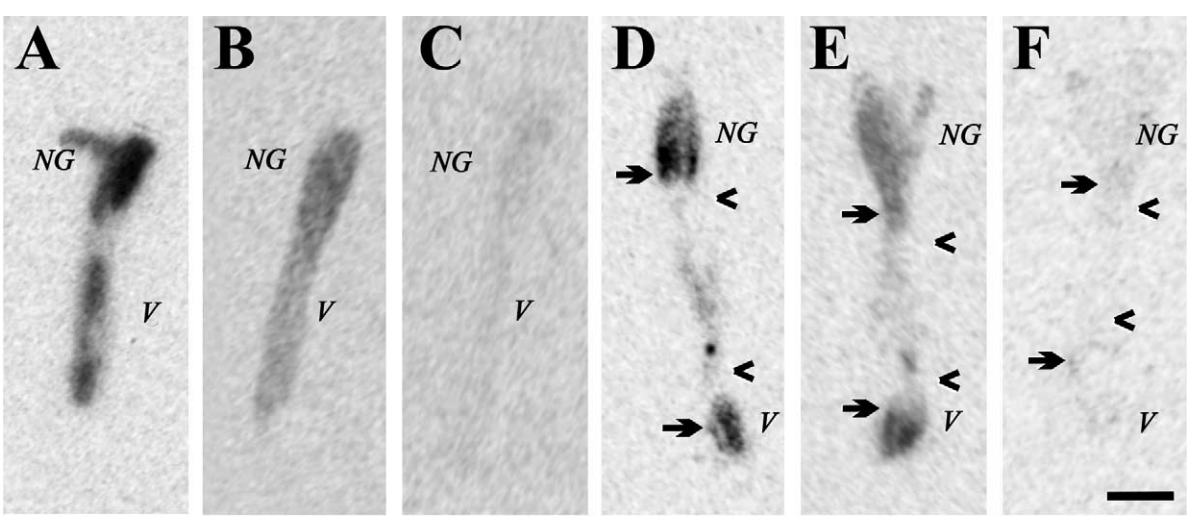

Fig. 2. Representative autoradiograms of [α^{33}P]dATP binding in the rat nodose ganglia (A–C) and vagal ligated preparations (D–F). (A) Autoradiogram of total binding of [α^{33}P]dATP on rat nodose ganglia (NG) and vagus nerve (V), showing intense binding over the nodose ganglion and lighter [α^{33}P]dATP binding can be seen along the vagus nerve. (B) Inclusion of α,βMeATP (100 μM), a P2X receptor agonist, failed to displace [α^{33}P]dATP binding. (C) Incubation with 2MeSATP (1 μM), a putative $P2Y_1$ receptor agonist, significantly inhibited the [α^{33}P]dATP binding, as determined by densitometric analysis. (D–F) Autoradiograms of nodose ganglia (NG) with distally vagal ligated trunks (V), white open arrows indicating the dual ligature sites and black arrows indicated the site of accumulation of [α^{33}P]dATP binding. Total binding of [α^{33}P]dATP clearly shows accumulation of [α^{33}P]dATP binding central to the proximal ligature and peripheral to the distal ligature (D), suggesting the bi-directional transport of [α^{33}P]dATP binding. Accumulation of [α^{33}P]dATP binding is clearly discernible in the presence of α,βMeADP (100 μM, E). Incubation with 2MeSATP (1 μM, F) significantly displaced the accumulation of [α^{33}P]dATP binding, as determined by densitometric analysis. Scale bar = 1 mm.

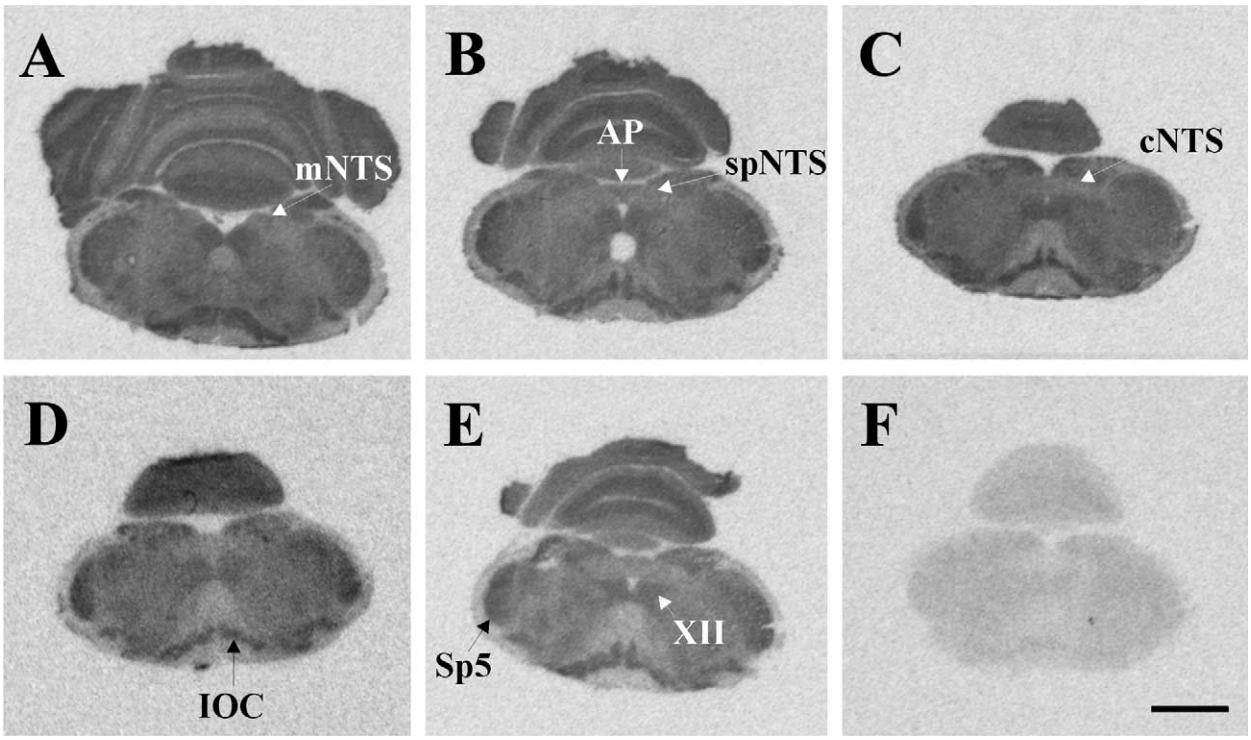

Fig. 3. Representative autoradiograms of [α^{33}P]dATP binding in rat brainstem sections, taken from the same animal, showing total binding (A–C) and binding in the presence of (D) α,βMeATP (100 μM), (E) α,βMeADP (100 μM), or (F) 2MeSATP (1 μM), on adjacent sections. (A–C) Binding of [α^{33}P]dATP can be seen in a number of brainstem regions, including the RVLM, CVLM and IOC. Low levels of [α^{33}P]dATP binding were apparent throughout the rostro-caudal extent of the NTS. [α^{33}P]dATP binding was unaltered in the presence of α,βMeATP (D) while inclusion of α,βMeADP (E) significantly inhibited [α^{33}P]dATP binding by ∼50%, and 2MeSATP (F) reduced binding of [α^{33}P]dATP by ∼70%, suggesting preferential binding of [α^{33}P]dATP to $P2Y_1$ receptors. Scale bar = 2 mm. Abbreviations: XII, hypoglossal; AP, area postrema; cNTS, commissural NTS; IOC, inferior olivary complex; mNTS, medial NTS; spNTS, subpostremal NTS; Sp5, spinal trigeminal nucleus.

Medulla oblongata. Binding of [α^{33}P]dATP was found in a number of other regions within the rat brainstem (Fig. 3A–C), including binding in both RVLM and CVLM, all subregions of the inferior olivary complex (IOC), hypoglossal nucleus, lateral reticular nucleus (LRt), spinal trigeminal nucleus (Sp5), gracile nucleus (Gr), cuneate nucleus (Cu) and external cuneate nucleus (ECu) (Table 3).

Table 2. Total binding, expressed as DPM/mm^2 and percentage of total [α^{33}P]dATP binding within the rat DVC in the presence of a number of displacers

Displacers	Conc. (M)	Regions			
		mNTS	spNTS	cNTS	AP
Total binding (DPM/mm^2)		356 ± 18	332 ± 14†	410 ± 17	293 ± 11
% Total binding:					
NECA	10 μM	120 ± 15	153 ± 11	137 ± 12	161 ± 44
PPADS	100 μM	113 ± 4	130 ± 14	109 ± 10	123 ± 14
NF279	1 μM	107 ± 16	113 ± 13	98 ± 4	116 ± 10
UTP	100 μM	81 ± 9	86 ± 4	77 ± 7	99 ± 11
α,βMeATP	100 μM	76 ± 9	97 ± 6	81 ± 5	104 ± 12
2MeSATP	1 μM	42 ± 4*	45 ± 4*	32 ± 4*	54 ± 5
α,βMeADP	100 μM	53 ± 3*	51 ± 4*	51 ± 2*	50 ± 4*
UTP	100 μM	2 ± 0.4*	3 ± 0.5*	2 ± 0.2*	1.6 ± 0.4*
α,βMeATP	100 μM				
2MeSATP	1 μM				
UTP	100 μM	1.3 ± 0.3*	0.9 ± 0.1*	1 ± 0.2*	0.3 ± 0.2*
α,βMeATP	100 μM				
2MeSATP	1 μM				
α,βMeADP	100 μM				

Data represent mean observations made over a minimum of four sections per displacer for each region in $n = 4$ rats.
†Comparison of total between spNTS and cNTS, one-way repeated measures ANOVA, post hoc Bonferroni's *t*-test, $P < 0.05$.
*Binding in the presence of displacer compared to total binding, calculated using DPM/mm^2. $P < 0.05$, one-way ANOVA, post hoc Bonferroni's *t*-test.

Table 3. Percentage of total [α^{33}P]dATP binding within the rat medulla oblongata in the presence of a number of displacers

Displacers	Conc. (M)	Regions							
		RVL	CVL	LRt	XII	IOC	Gr	Cu	Sp5
Total binding (DPM/mm^2)		479 ± 28	467 ± 27	468 ± 35	467 ± 13	466 ± 33	463 ± 20	497 ± 19	484 ± 13
% Total binding:									
NECA	10 μM	134 ± 14	146 ± 17	137 ± 12	145 ± 15	150 ± 10	139 ± 17	157 ± 10	145 ± 9
PPADS	100 μM	106 ± 4	116 ± 7	115 ± 6	109 ± 7	108 ± 2	101 ± 6	125 ± 15	109 ± 7
NF279	1 μM	103 ± 5	106 ± 8	106 ± 10	102 ± 6	103 ± 1	92 ± 3	107 ± 9	100 ± 5
UTP	100 μM	73 ± 6	85 ± 6	81 ± 7	82 ± 9	81 ± 7	68 ± 5	78 ± 9	72 ± 6
α,βMeATP	100 μM	85 ± 2	90 ± 3	85 ± 4	85 ± 4	76 ± 3	79 ± 4	95 ± 7	82 ± 4
2MeSATP	1 μM	17 ± 2*	17 ± 1*	16 ± 1*	30 ± 3*	28 ± 4*	26 ± 3*	22 ± 2*	24 ± 3*
α,βMeADP	100 μM	52 ± 5*	53 ± 2*	51 ± 4*	58 ± 2*	52 ± 2*	55 ± 3*	59 ± 1*	58 ± 4*
UTP	100 μM	2 ± 0.3*	2 ± 0.1*	1 ± 0.1*	2 ± 0.4*	2 ± 0.4*	2 ± 0.2*	3 ± 0.3*	3 ± 0.1*
α,βMeATP	100 μM								
2MeSATP	1 μM								
UTP	100 μM	0.7 ± 0.2*	1 ± 0.3*	0.7 ± 0.1*	1.3 ± 0.4*	1 ± 0.2*	1 ± 0.2*	1.8 ± 0.2*	1.3 ± 0.3*
α,βMeATP	100 μM								
2MeSATP	1 μM								
α,βMeADP	100 μM								

*Binding in the presence of displacer compared to total binding, calculated using DPM/mm^2. $P < 0.05$, one-way ANOVA, Bonferroni's *t*-test post hoc.
Data represent mean observations made over a minimum of six sections per displacer for each region in $n = 4$ rats.

Displacement of binding by inclusion of various receptor agonists and antagonists yielded similar results to that seen in the DVC, with complete displacement by ATP. Inclusion of NECA potentiated binding between 45% and 82.5%, within most nuclei examined (Table 3). However, a significant difference was only observed in Cu (+61.5%) and ECu (+82.5%). PPADS did not significantly alter the binding of [α^{33}P]dATP in any region examined, though a trend towards potentiation (up to +30%) was seen in all regions; most notably in the Cu and ECu, both having ~25% increase in binding over total binding (Table 3). Similarly, NF279 did not significantly alter the level of binding within the regions examined (Table 3). Inclusion of UTP did not produce significant inhibition of [α^{33}P]dATP binding, though an average of ~24% inhibition of binding was seen in all regions (Table 3). Incubation in the presence of α,βMeATP resulted in no significant inhibition of binding in all regions examined, with a maximum of −23% inhibition, seen in the IOC (Table 3, Fig. 3D). Incubation with α,βMeADP resulted in a significant inhibition of ~45%, compared to total binding, in all regions examined (Table 3), furthermore, less background binding was apparent on the autoradiograms (Fig. 3E). In addition, significant inhibition by 2MeSATP of [α^{33}P]dATP binding was found in all nuclei examined (Table 3, Fig. 3F). Displacement by a combination of agonists (UTP, α,βMeATP and 2MeSATP) in the presence or absence of α,βMeADP both resulted in significant inhibition of binding in all regions. Levels of binding in all regions in the presence of these 'cocktails' were barely distinguishable from background (Table 3).

$P2Y_1$ receptor immunohistochemistry

Antisera specificity. The antisera used in the present study were characterised as shown in Fig. 1. A western blot using the $P2Y_1$ antibody resulted in a major band of 65 kDa (Fig. 4A), whereas pre-absorption with the conjugated peptide epitope abolished the band at this molecular weight (Fig. 4B). Pre-adsorption of the conjugated peptide epitope also prevented the visualisation of IR in rat tail artery and in rat midbrain following subsequent incubation with $P2Y_1$ antisera (Fig. 4C–F). A dilution curve in rat brain slices indicated that a dilution of 1/3000 resulted in reproducible IR with minimal background staining. Omission of either primary or secondary antisera resulted in a lack of reaction product (Fig. 4E, F).

$P2Y_1$-IR in rat nodose ganglia: effect of vagal ligation. Ligation of the rat vagus nerve resulted in a clear accumulation of $P2Y_1$-IR (Fig. 5A, B) and $P2X_2$-IR (Fig. 5C) adjacent to both ligatures. Accumulation of immunoreactive product was found central to the proximal ligature and peripheral to the distal ligature, suggesting anterograde and retrograde transport, respectively. Cells and fibres immunopositive to $P2Y_1$-IR and $P2X_2$-IR were clearly evident in the nodose ganglion.

$P2Y_1$-IR in rat medulla

DVC. Immunopositive cells and fibres were evidenced throughout the DVC (Fig. 6), and were particularly dense in the AP, the border of AP and the Gr (Fig. 6D), and throughout the entire extent of the NTS (Fig. 6). $P2Y_1$ receptor-IR was typically more dense in regions of the NTS medial of the solitary tract (Fig. 6E, F), however, the number of $P2Y_1$-IR cells lateral to the tract tended to increase in a rostral direction. In addition, $P2Y_1$-IR was visualised within the solitary tract (Fig. 6F). Neurones in the dorsal motor nucleus of the vagus (DMX) were also immunoreactive to the $P2Y_1$ antisera, particularly at more rostral levels (Fig. 6E, F). Figure 6 depicts the distribution of $P2Y_1$-IR throughout

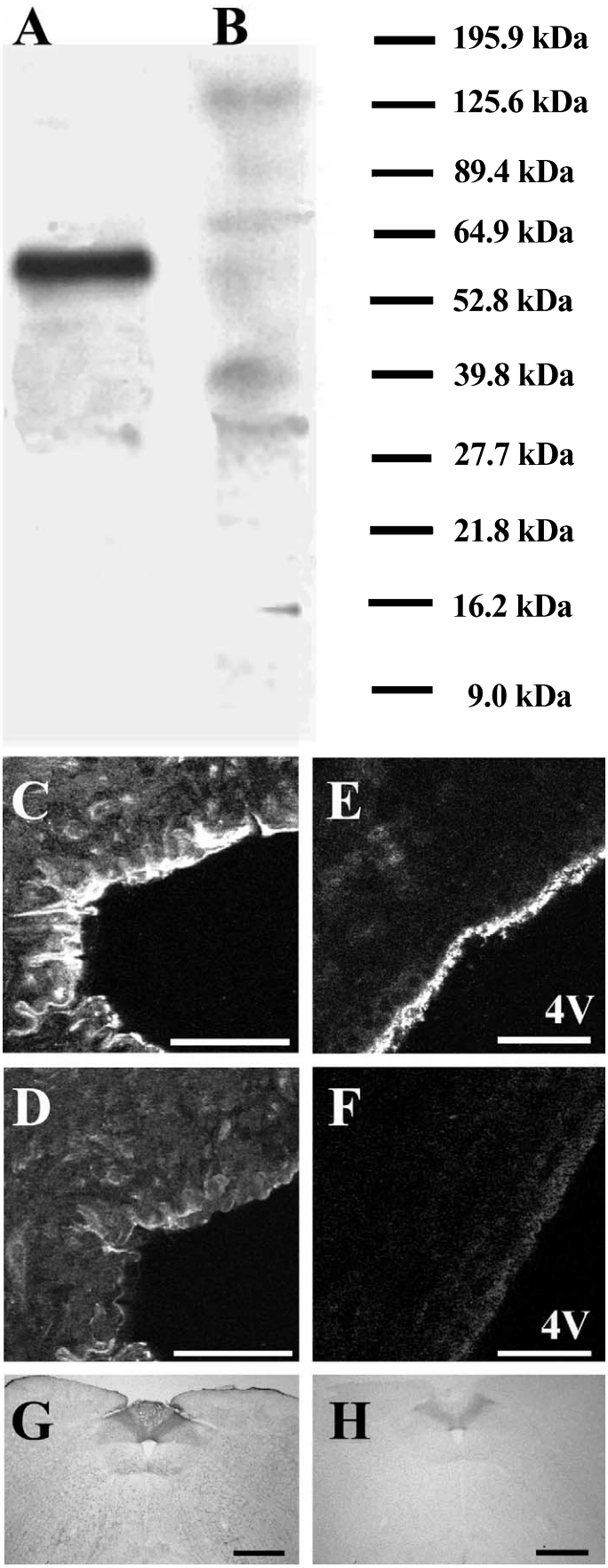
A
B
195.9 kDa
125.6 kDa
89.4 kDa
64.9 kDa
52.8 kDa
39.8 kDa
27.7 kDa
21.8 kDa
16.2 kDa
9.0 kDa
C
E
4V
D
F
4V
G
H

Fig. 4.

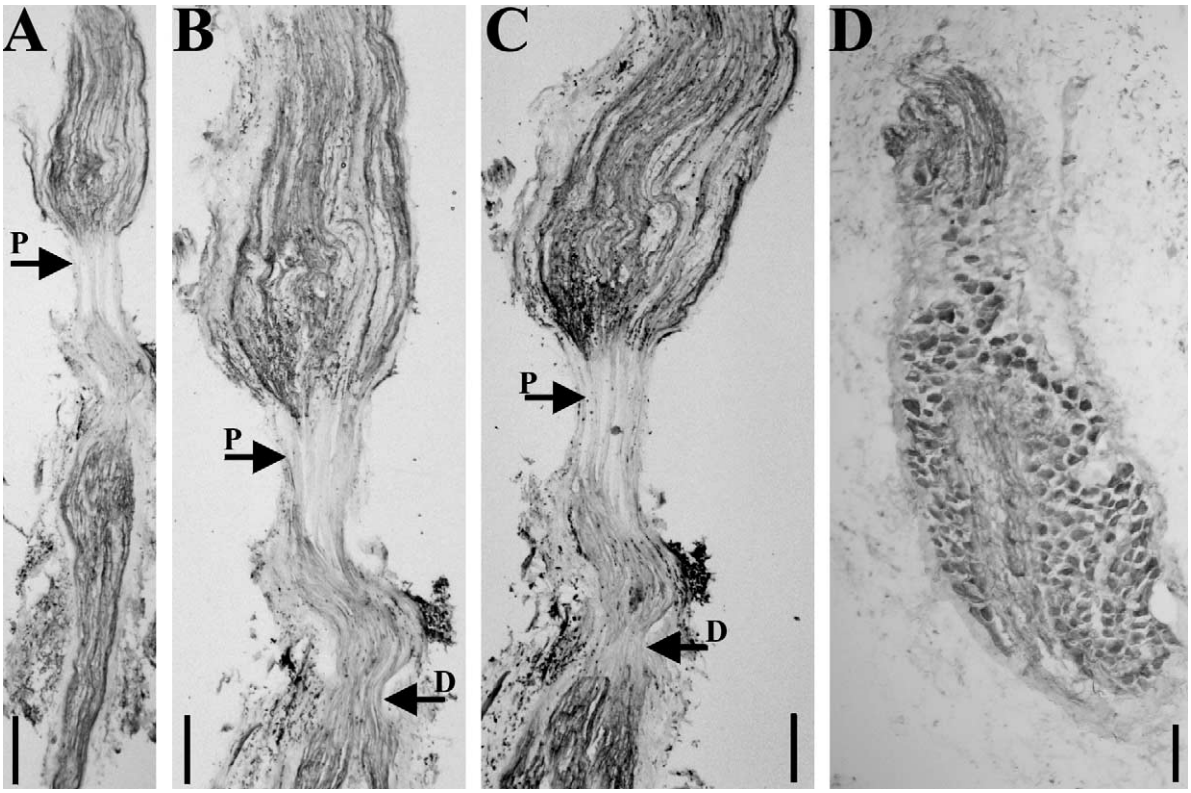

Fig. 5. Photomicrographs of P2Y$_1$-IR and P2X$_2$-IR receptor within the rat vagus nerve following unilateral vagal ligation. (A, B) Accumulation of P2Y$_1$-IR receptor following ligation of the vagus nerve using two ligatures. (A) P2Y$_1$ immunoreactive product is clearly apparent adjacent to the proximal (P) ligature. Scale bar = 500 μm. (B) P2Y$_1$-IR antiserum is discernible proximal to the proximal ligature (P) and distal to the distal ligature (D), suggesting bi-directional transport of the P2Y$_1$ receptor. Scale bar = 250 μm. (C) P2X$_2$-IR receptor accumulation is clearly apparent proximal to the proximal ligature and distal to the distal ligature. Scale bar = 250 μm. (D) P2Y$_1$-IR receptor associated with vagal perikarya and fibres passing through the rat nodose ganglion. Scale bar = 100 μm.

the rat DVC, while semi-quantitative data are given in Table 4.

Medulla oblongata. Immunostaining for the P2Y$_1$ receptor subtype was found widely distributed throughout the rat brainstem, with a clear topographic profile (Table 5). The most striking presence of P2Y$_1$-IR cells was within the hypoglossal nucleus, immediately ventral of the DMX and bordering the central canal/fourth ventricle. Dense neuropil staining was also observed in the hypoglossal nucleus (Fig. 7B). In addition, the ventral region of the Gr contained a dense cluster of P2Y$_1$-IR cells, often with complex dendritic arborisations (Fig. 7A). Cells immunopositive to the P2Y$_1$ receptor were also found in the LRt of the medulla (Fig. 7C) and in the CVLM. The medullary reticular formation contained a scattering of immunoreactive neurones throughout all subregions. Similarly, the Sp5 and the IOC demonstrated relatively low levels of P2Y$_1$-IR, both cells and fibres. As evidenced in the DMX, the parasympathetic efferent neurones of nucleus ambiguus were also P2Y$_1$-IR, which was clearly apparent in the compact formation (Fig. 7D). P2Y$_1$-IR neurones were also visualised ventral of nucleus ambiguus, in the RVLM and medially within the rostral ventral medial medulla (RVMM). These cells typically demonstrated substantial dendritic IR (Fig. 7F). The midline raphe nuclei exhibited a relatively dense distribution of immunostained cells (Fig. 7E).

DISCUSSION

The current study provides the first clear evidence of widespread P2Y$_1$-IR receptor in the adult rat medulla

Fig. 4. Characterisation of P2Y$_1$ antisera specificity. (A, B) Lane A shows a western blot using P2Y$_1$ antibody, showing a major band at the approximate molecular weight of 65 kDa. Lane B shows a western blot following pre-absorption with the conjugated peptide epitope (10 μM). (C, D) Adjacent sections of rat tail artery. Scale bar = 50 μm. (C) Incubated with the P2Y$_1$ antisera, demonstrating clear IR in the endothelium, visualised with Cy3. (D) In an adjacent section, pre-incubated with epitope peptide conjugate (10 μM) which prevents visualisation of IR following subsequent addition of the P2Y$_1$ antisera. (E, F) Adjacent sections of rat midbrain. Scale bar = 50 μm. (E) Incubated with the P2Y$_1$ antisera, demonstrating clear IR in the ependymal cells bordering the fourth ventricle (4V) visualised with Cy3. (F) In an adjacent section, pre-incubation with epitope peptide conjugate (10 μM) prevents visualisation of IR following subsequent addition of the P2Y$_1$ antisera. (G) Photomicrograph of section of rat brainstem, incubated with P2Y$_1$ antisera, and in the absence of the P2Y$_1$ antisera (H). IR to the P2Y$_1$ antisera was particularly apparent within the DVC (G). Omission of the P2Y$_1$ antisera resulted in a lack of reaction product over neurones (H). Scale bar = 1 mm.

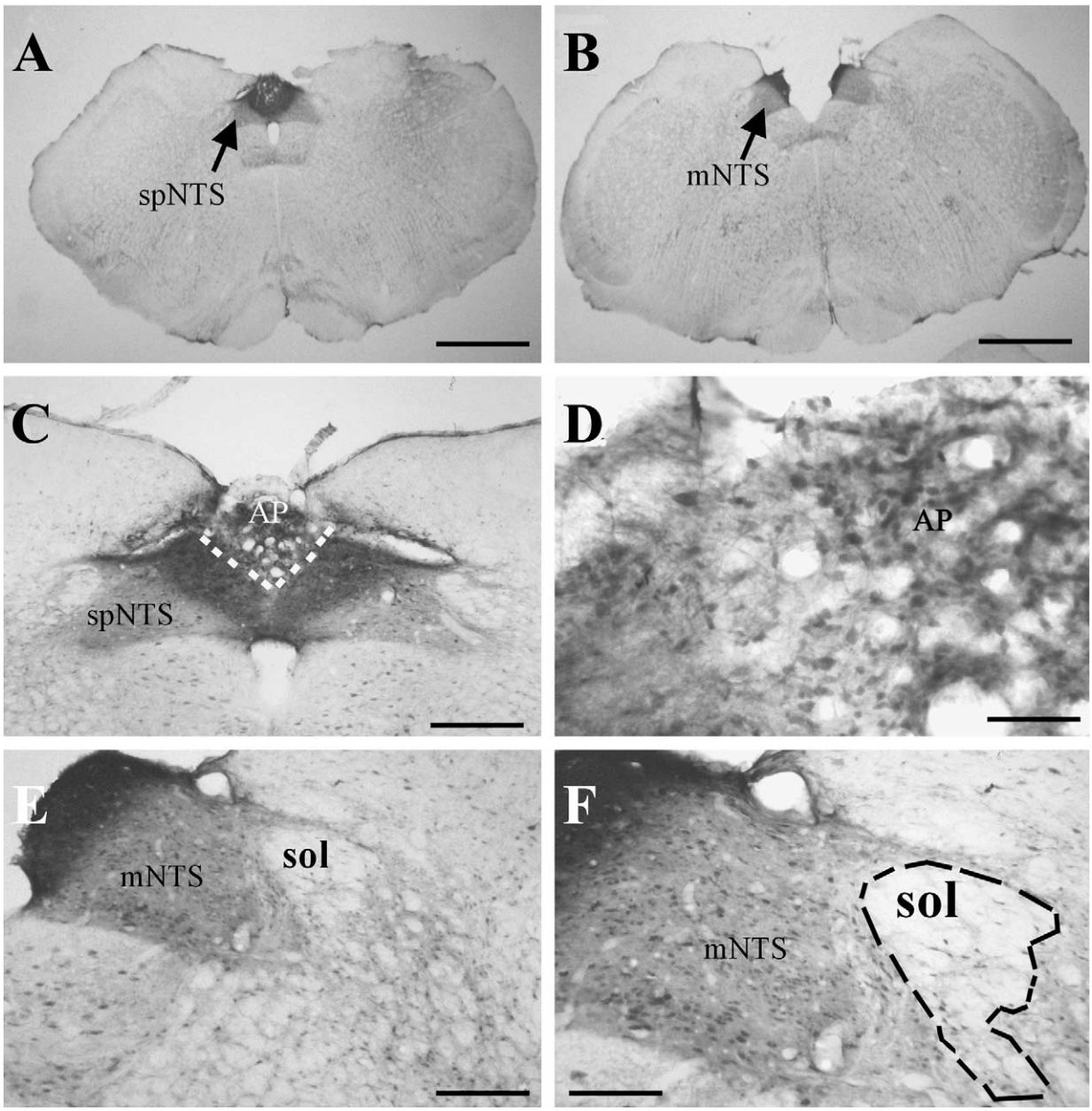

Fig. 6. Photomicrographs of $P2Y_1$-IR receptor within the rat DVC. Whole slice of rat medulla oblongata, at the level of the spNTS (A) and mNTS (B), showing dense reaction product in the NTS relative to other regions. Scale bar = 2 mm. (C) DVC, showing dense reaction product evident in the AP and the spNTS, particularly medial of the solitary tract. Scale bar = 1 mm. (D) AP, clearly containing a dense cluster of immunoreactive cells, and a plexus of fibres. Scale bar = 0.1 mm. (E) mNTS, demonstrating a gradient of $P2Y_1$-IR between the medial and lateral subregions of the NTS, with binding more apparent medial of the solitary tract (sol). Scale bar = 0.5 mm. (F) Magnification of (E), demonstrating neuropil staining within the mNTS, and dense staining of the motor neurones within the DMX. In addition, $P2Y_1$-IR is evident within the solitary tract (sol). Scale bar = 0.2 mm.

oblongata; furthermore, this $P2Y_1$-IR is also subject to bi-directional transport along the rat vagus nerve. In addition, observations from this study suggest the potential use of [α^{33}P]dATP as a radioligand for P2Y receptor autoradiography. Taken together, our observations further extend the findings of previous autoradiographic studies, which identified a number of P2Y-like binding sites throughout the chick and rat brain (Simon et al., 1997; Webb et al., 1998), although doubts have been raised over the specificity of [^{35}S]dATPαS as an appropriate radioligand (Schachter and Harden, 1997), since dATPαS may also have agonist activity at P2X receptors (Pubill et al., 2001), and also $P2Y_1$-IR in the rat brain (Moran-Jimenez and Matute, 2000). In combination with previous observations, the widespread distribution of P2X receptors within both the rat and primate brainstem (Yao et al., 2000), and the present demonstration of $P2Y_1$ receptors, provide mounting evidence for the likely role of purinergic neurotransmission in central autonomic regulation.

Table 4. Semi-quantitation of P2Y$_1$-IR receptor in rat DVC

Brain region	Cells	Fibres
AP	++++	present
cNTS, lateral	+++	present
cNTS, medial	++++	present
spNTS	++++	present
mNTS, lateral	+++	present
mNTS, medial	++++	present

The number of labelled cell bodies throughout the brainstem were scored in the following manner: 0 cells (−), <10 cells (+), 10–19 cells (++), 20–49 cells (+++), >50 cells (++++). Data represent the mean of observations made throughout the extent of the medulla in $n=6$ rats.

Observations from the current study indicate that [α^{33}P]dATP binds to P2 receptors and not P1 receptors, as binding was completely displaced by excess ATP but remained unaltered in the presence of the non-selective P1 receptor agonist, NECA. While there appears to be a component of [α^{33}P]dATP binding to endogenous ecto-5′-nucleotidase, almost all binding could be displaced by a mixture of receptor agonists. The binding of [α^{33}P]dATP was insensitive to displacement by (i) UTP, an agonist at uracil selective P2Y receptors (von Kügelgen and Wetter, 2000) at a 100-fold higher concentration than 2MeSATP; (ii) α,βMeATP, a P2X receptor agonist; (iii) PPADS, a non-selective P2 receptor antagonist; (iv) NF279, P2X$_1$ receptor antagonist (Ralevic and Burnstock, 1998). In addition, the binding of [α^{33}P]dATP can be accounted for by 2MeSATP (∼70% inhibition) and α,βMeADP (∼50%). Moreover, the similarities between brainstem regions containing P2Y$_1$-IR receptor antibody and [α^{33}P]dATP binding suggest that the radioligand may bind to P2Y$_1$ receptors. It is clearly possible however that [α^{33}P]dATP may also label P2Y$_{11}$ receptors, since dATP has agonist activity at P2Y$_{11}$ receptors (Communi et al., 1999) and the mRNA encoding this receptor has recently been demonstrated in human medulla oblongata (Moore et al., 2001) and canine brain (Zambon et al., 2001), although in this instance only cortex and cerebellum were analysed. The absolute confirmation of the degree of binding to various P2 receptor subtypes awaits further clarification, with the use of subtype selective tools. This will be aided by compounds such as MRS2179 (Boyer et al., 1998; Baurand et al., 2001) and benzoyl ATP (Vigne et al., 1999), selective P2Y$_1$ receptor antagonists. For technical considerations, images obtained from incubation with α,βMeADP provided a clearer resolution of individual nuclei, due to the removal of background binding to endogenous ecto-5′-nucleotidase, suggesting that this compound should routinely be included in the incubation mixture in future experiments.

A significant difference in [α^{33}P]dATP binding was seen between the rat and human nodose ganglia. While binding was sensitive to 2MeSATP, in both the rat and human nodose ganglia, α,βMeATP was also able to significantly displace [α^{33}P]dATP binding in the human ganglia. These differences may represent a species difference in distribution and function of P2 receptors but may also indicate that α,βMeATP fails to retain its selectivity in human tissue. Previous study has illustrated differences in distribution of P2X$_2$ and P2X$_3$ receptors between rat and monkey (Vulchanova et al., 1997), thus data from this study may indicate further differences between the purinergic receptors between species. Alternatively, it is clearly possible that in human inferior vagal ganglia, [α^{33}P]dATP binds to P2X$_4$ and/or P2X$_6$ receptors, that would not be displaced by PPADS or the selective P2X$_1$ receptor antagonist, NF279 (Klapperstuck et al., 2000; Rettinger et al., 2000); however, confirmation of this awaits the development of P2X$_{4/6}$ selective ligands.

Incubation with PPADS, non-selective P2 receptor antagonist, showed an apparent potentiation of [α^{33}P]dATP binding within the rat brainstem and nodose ganglia. The exact reason for this phenomenon is currently unknown, but may reflect allosteric modulation of binding to metabotropic receptors, resulting in increased ligand binding. Similarly, the decreased binding in the presence of α,βMeATP may not be due to direct displacement, but rather an equivalent mechanism, where the activation of P2X receptor reduces the function or affinity of the P2Y receptor, resulting in a reduction in [α^{33}P]dATP binding. No change was observed in the presence of NF279, a putative P2X$_1$ receptor antagonist, suggesting this mechanism requires the participation of more than one receptor subtype. At this point, the exact mechanism of the effect of PPADS is unclear since PPADS has also been shown to antagonise P2Y$_1$ receptors (Lambrecht, 1996), thus a definitive answer to this observation awaits the availability of a range of subtype selective antagonists.

Similar to PPADS, an apparent potentiation was also seen in the presence of NECA, a non-selective P1 receptor agonist (Ralevic and Burnstock, 1998), though this was not significant a clear trend was observed. The adenosine (P1) receptors are G protein-coupled receptors, with seven transmembrane domains, thus far, four distinct subtypes, A$_1$, A$_{2A}$, A$_{2B}$, A$_3$, have been characterised (Fredholm et al., 1994). Whilst the mRNA for all four receptor subtypes has been identified within the

Table 5. Semi-quantitation of P2Y$_1$-IR receptor in rat medulla oblongata

Brain region	Cells	Fibres
Cu	++	present
Gr	+++	present
Hypoglossal nucleus	++++	present
Sp5	scattered throughout	present
LRt	+++	present
Nucleus ambiguus	++	present
CVLM	++	present
RVLM	+++	present
Reticular formation	scattered throughout	present
Raphe obscurus/magnus	++	present
IOC	scattered throughout	present

The number of labelled cell bodies throughout the brainstem were scored in the following manner: 0 cells (−), <10 cells (+), 10–19 cells (++), 20–49 cells (+++), >50 cells (++++). Data represent the mean of observations made throughout the extent of the medulla in $n=6$ rats.

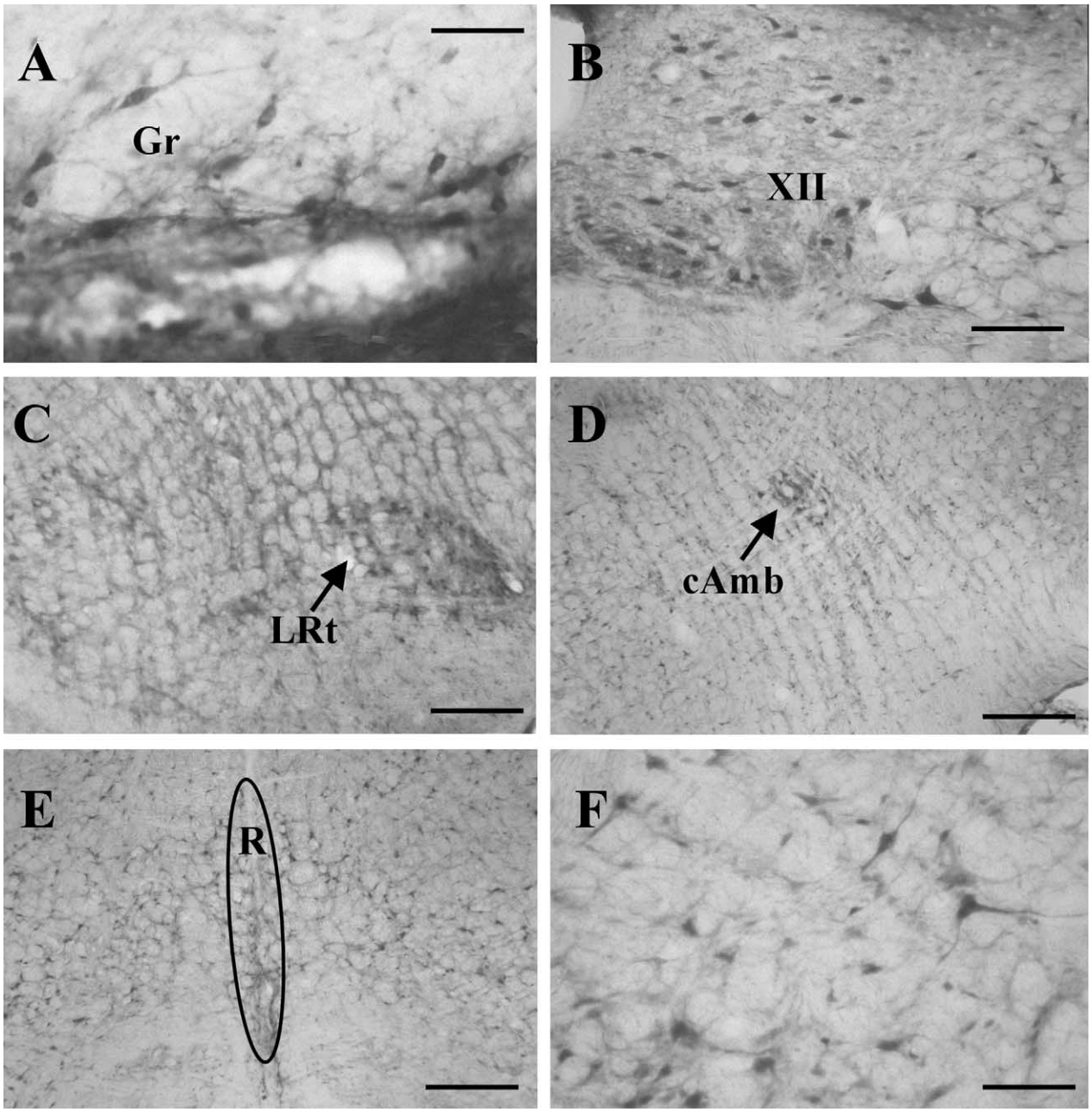

Fig. 7. Photomicrographs of $P2Y_1$-IR receptor throughout the rat medulla oblongata. (A) Ventral region of the Gr, bordering AP. Scale bar = 0.1 mm. (B) Hypoglossal nucleus (XII), exhibiting $P2Y_1$-IR in neurones and neuropil. Scale bar = 0.2 mm. (C) LRt. Scale bar = 0.2 mm. (D) Compact formation of nucleus ambiguus (cAmb). Scale bar = 0.5 mm. (E) Midline raphe (R). Scale bar = 0.5 mm. (F) Rostral ventromedial medulla. Scale bar = 0.1 mm.

brain, the A_1 receptor appears to be particularly ubiquitous throughout the rat brain, with high levels of expression throughout much of the brain, including the brainstem (Dixon et al., 1996). Immunohistochemical (Rivkees et al., 1995), membrane binding (Krstew et al., 1998) and autoradiographic (St Lambert et al., 1996) studies have shown heavy labeling of A_1 receptors within the brainstem, similar to the distribution of [α^{33}P]dATP binding seen in the present study, including the ventrolateral medulla and NTS. The potentiation of [α^{33}P]dATP binding in the presence of NECA suggests a possible positive interaction between the A_1 and $P2Y_1$ receptor systems. A number of studies have indicated synergistic interactions between A_1 receptors and other G protein-coupled receptors, typically pertussis toxin insensitive $G_{q/11}$ proteins, including between A_1 and α_1 adrenoceptors (Haggblad and Fredholm, 1987), H_1 histamine receptors (Dickenson and Hill, 1994) and ATP (Megson et al., 1995). Evidence exists to indicate that A_1 adenosine receptors can clearly interact with a large number of other transmitter systems, this opens the possibility of a potential positive interaction between the A_1 and $P2Y_1$ receptors. Interestingly, a recent report has demonstrated the ability of A_1 and $P2Y_1$ receptors to form a heteromeric receptor complex (Yoshioka et al., 2001). In such co-expressed receptors, the affinity of the

$P2Y_1$ agonist ADPβS was increased 400-fold. However, further study is required to elucidate whether this interaction is occurring on brain slices under the present conditions.

The technique of vagal ligation has been widely used to study the axonal transport of receptors, transporters and enzymes, such as bradykinin receptors (Krstew et al., 1998), adenosine transporters (Castillo-Melendez et al., 1996b) and nitric oxide synthase (Fong et al., 2000; Lumme et al., 1996). In the current study, the ligation of the vagus nerve using two ligatures resulted in the accumulation of both $P2Y_1$-IR and [α^{33}P]dATP binding adjacent to both ligatures; central to the proximal ligature and peripheral to the distal ligature. In addition, the accumulation of [α^{33}P]dATP binding adjacent to vagal ligations was also specifically displaced by 2MeSATP, suggesting the bi-directional transport of P2Y receptors. Similarly, $P2Y_1$-IR and $P2X_2$-IR were also seen to accumulate adjacent to both ligatures. $P2X_2$ receptors have been previously shown to be present on the nodose ganglia (Collo et al., 1996; Virginio et al., 1998; Vulchanova et al., 1997; Xiang et al., 1998), and within vagal afferent terminals in the NTS (Atkinson et al., 2000). In addition, Vulchanova et al. (1996) showed that this IR was abolished following nodose ganglionectomy, suggesting that the $P2X_2$-IR within the NTS originated from the nodose ganglion. The current study has shown, for the first time, direct evidence that the $P2X_2$ receptor is subject to bi-directional transport along the rat vagus nerve. We also demonstrate clear evidence of bi-directional transport of $P2Y_1$-IR along the rat vagus nerve. The possibility of presynaptic $P2Y_1$ receptors at vagal terminals in the NTS is further supported by this finding and the visualisation of $P2Y_1$-IR within the solitary tract. There was no indication of any change in either [α^{33}P]dATP binding or $P2Y_1$-IR following unilateral vagal ligation in the NTS; however, since the ligatures were secured on the peripheral side of the nodose ganglion, afferent terminals in the NTS should be relatively unchanged.

The current study also reports the first description of $P2Y_1$-IR throughout the rat medulla oblongata. The antiserum employed was characterised by western blot, demonstrating an apparent molecular weight of ~65 kDa, consistent with other antisera directed against this receptor (Moore et al., 2000). This form represents a modified (glycosylated) receptor, rather than the native protein. Furthermore, pre-absorption of rodent arterial and brain tissue with the conjugated peptide epitope abolished IR. Omission of the primary antibody in slices of rat brainstem resulted in a lack of reaction product, with the exception of a degree of peroxidase activity apparently associated with tanycytic processes in the border between the AP and NTS.

A most notable region containing $P2Y_1$-IR was the NTS, a key relay site for afferent viscerosensory input to the CNS. The present study focused on the subpostremal and medial subregions of the NTS, areas linked to central cardiovascular control mechanisms and terminations of arterial baro- and chemoreceptor afferents (Lawrence and Jarrott, 1996). Furthermore, IR was particularly prominent medial of the solitary tract. Considerable evidence exists detailing the involvement of purines in central cardiovascular and respiratory control, especially at the level of the NTS (Barraco et al., 1991, 1996; Castillo-Melendez et al., 1996a,b; Ergene et al., 1994; Lawrence and Jarrott, 1996; Scislo et al., 1998; Scislo and O'Leary, 2000; Thomas and Spyer, 2000), however, pharmacological characterisation of receptor subtypes has been hampered by the lack of appropriate tools. Current information suggests that $P2Y_1$ receptors may indeed play a role in central cardiovascular modulation, in addition to P2X receptors. A number of studies have demonstrated P2X receptor involvement in the baroreflex in the NTS, as intra-NTS administration of suramin markedly impairs baroreflex function in anaesthetised rats (Scislo et al., 1998), implicating P2X receptors in reflex bradycardia function. However, though generally regarded as a P2X receptor antagonist, suramin has been demonstrated to be an antagonist at $P2Y_1$ receptors, thus this effect of suramin may include some action on the $P2Y_1$ receptors. Intra-NTS administration of 2MeSATP has also been shown to cause potent depressor and bradycardic responses, similar in magnitude to those elicited by ATP (Ergene et al., 1994). In addition, we have demonstrated both $P2Y_1$-IR and binding of [α^{33}P]dATP, displaceable by 2MeSATP, within the NTS and the solitary tract. Furthermore, both the $P2Y_1$-IR and [α^{33}P]dATP binding was transported bi-directionally along the rat vagus nerve, consistent with the location of $P2Y_1$ receptors on vagal afferent terminals within the spNTS and the medial NTS (mNTS). Studies at the electron microscope level will unequivocally determine whether or not $P2Y_1$ receptors occur on central terminals of vagal afferents. Modulation of transmitter release by presynaptic P2Y receptors has been previously demonstrated in A6 neurones (Poelchen et al., 1999) and remains to be shown within the NTS.

In addition to the NTS, $P2Y_1$-IR was also present within neurones in the DMX and the compact formation of nucleus ambiguus. Such an observation would be consistent with the presence of $P2Y_1$ receptors on efferent vagal motor neurones innervating the viscera. The large motor neurones of the hypoglossal nucleus also displayed prominent $P2Y_1$-IR and dense [α^{33}P]dATP binding. ATP has been shown to excite hypoglossal neurones, thereby modulating inspiratory activity and hypoglossal motor outflow (Funk et al., 1997). These data suggest that $P2Y_1$ receptors may have a role in the modulation of hypoglossal activity.

In conclusion, these data indicate the potential for neuromodulation by the G protein-linked $P2Y_1$ receptors within the rat brainstem. In addition, we have demonstrated for the first time the potential use of [α^{33}P]dATP as a radioligand for the study of P2(Y) receptors. The precise functional role of P2-purinoceptors in central autonomic regulation awaits the further development of subtype selective pharmacological tools.

Acknowledgements—These studies were supported in part by the National Health and Medical Research Council of Australia, of which A.J.L. is an R.D. Wright Fellow.

REFERENCES

Atkinson, L., Batten, T.F., Deuchars, J., 2000. $P2X_2$ receptor immunoreactivity in the dorsal vagal complex and area postrema of the rat. Neuroscience 99, 683–696.

Barraco, R.A., El-Ridi, M.R., Ergeen, E., Phillis, J.W., 1991. Adenosine receptor subtypes in the brainstem mediate distinct cardiovascular response patterns. Brain Res. Bull. 26, 59–84.

Barraco, R.A., O'Leary, D.S., Ergene, E., Scislo, T.J., 1996. Activation of purinergic receptor subtypes in the nucleus tractus solitarius elicits specific regional vascular response patterns. J. Auton. Nerv. Syst. 59, 113–124.

Baurand, A., Raboisson, P., Freund, M., Leon, C., Cazenave, J.P., Bourguignon, J.J., Gachet, C., 2001. Inhibition of platelet function by administration of MRS2179, a $P2Y_1$ receptor antagonist. Eur. J. Pharmacol. 412, 213–221.

Boyer, J.L., Delaney, S.M., Villaneuva, D., Harden, T.K., 2000. A molecularly identified P2Y receptor simultaneously activates phospholipase C and inhibits adenylyl cyclase and is nonselectively activated by all nucleoside triphosphates. Mol. Pharmacol. 57, 805–810.

Boyer, J.L., Mohanram, A., Camaioni, E., Jacobson, K.A., Harden, T.K., 1998. Competitive and selective antagonism of $P2Y_1$ receptors by N^6-methyl 2′-deoxyadenosine 3′,5′-bisphosphate. Br. J. Pharmacol. 124, 1–3.

Boyer, J.L., Romero-Avila, T., Schachter, J.B., Harden, T.K., 1996. Identification of competitive antagonists of the $P2Y_1$ receptor. Mol. Pharmacol. 50, 1323–1329.

Burnstock, G., 1995. Noradrenaline and ATP: cotransmitters and neuromodulators. J. Physiol. Pharmacol. 46, 365–384.

Castillo-Melendez, M., Jarrott, B., Lawrence, A.J., 1996a. Markers of adenosine removal in normotensive and hypertensive rat nervous tissue. Hypertension 28, 1026–1033.

Castillo-Melendez, M., Jarrott, B., Lawrence, A.J., 1996b. Radioligand binding and autoradiographic visualization of adenosine transport sites in human inferior vagal ganglia and their axonal transport along rat vagal afferent neurons. J. Auton. Nerv. Syst. 57, 36–42.

Collo, G., North, R.A., Kawashima, E., Merlopich, E., Neidhart, S., Surprenant, A., Buell, G., 1996. Cloning of $P2X_5$ and $P2X_6$ receptors and the distribution and properties of an extended family of ATP-gated ion channels. J. Neurosci. 16, 2495–2507.

Communi, D., Gonzalez, N.S., Detheux, M., Brezillon, S., Lannoy, V., Parmentier, M., Boeynaems, J.M., 2001. Identification of a novel human ADP receptor coupled to Gi. J. Biol. Chem. 44, 41479–41485.

Communi, D., Robay, B., Boeynaems, J.M., 1999. Pharmacological characterization of the human $P2Y_{11}$ receptor. Br. J. Pharmacol. 128, 1199–1206.

Dickenson, J.M., Hill, S.J., 1994. Interactions between adenosine A_1- and histamine H_1-receptors. Int. J. Biochem. 26, 959–969.

Dixon, A.K., Gubitz, A.K., Sirinathsinghji, D.J., Richardson, P.J., Freeman, T.C., 1996. Tissue distribution of adenosine receptor mRNAs in the rat. Br. J. Pharmacol. 118, 1461–1468.

Edwards, F.A., Gibb, A.J., Colquhoun, D., 1992. ATP receptor-mediated synaptic currents in the central nervous system. Nature 359, 144–147.

Ergene, E., Dunbar, J.C., O'Leary, D.S., Barraco, R.A., 1994. Activation of P2-purinoceptors in the nucleus tractus solitarius mediate depressor responses. Neurosci. Lett. 174, 188–192.

Evans, R.J., Derkach, V., Surprenant, A., 1992. ATP mediates fast synaptic transmission in mammalian neurons. Nature 357, 503–505.

Filippov, A.K., Brown, D.A., Barnard, E.A., 2000. The $P2Y_1$ receptor closes the N-type Ca^{2+} channel in neurones, with both adenosine triphosphates and diphosphates as potent agonists. Br. J. Pharmacol. 129, 1063–1066.

Fong, A.Y., Talman, W.T., Lawrence, A.J., 2000. Axonal transport of NADPH-diaphorase and [^{3}H]nitro-L-arginine binding, but not [^{3}H]cGMP binding, by the rat vagus nerve. Brain Res. 878, 240–246.

Fredholm, B., Abbracchio, M., Burnstock, G., Daly, J., Harden, K., Joacobson, K., Leff, P., Williams, M., 1994. Nomenclature and classification of purinoceptors. Pharmacol. Rev. 46, 143–156.

Funk, G.D., Kanjhan, R., Walsh, C., Lipski, J., Comer, A.M., Parkis, M.A., Housley, G.D., 1997. P2 receptor excitation of rodent hypoglossal motoneuron activity *in vitro* and *in vivo*: a molecular physiological analysis. J. Neurosci. 17, 6325–6337.

Haggblad, J., Fredholm, B.B., 1987. Adenosine and neuropeptide Y enhance alpha 1-adrenoceptor-induced accumulation of inositol phosphates and attenuate forskolin-induced accumulation of cyclic AMP in rat vas deferens. Neurosci. Lett. 82, 211–216.

Hollopeter, G., Jantzen, H.M., Vincent, D., Li, G., England, L., Ramakrishnan, V., Yang, R.B., Nurden, A., Julius, D., Conley, P.B., 2001. Identification of the platelet ADP receptor targeted by antithrombotic drugs. Nature 409, 202–207.

Horiuchi, J., Potts, P.D., Tagawa, T., Dampney, R.A.L., 1999. Effects of activation and blockade of P2X receptors in the ventrolateral medulla on arterial pressure and sympathetic activity. J. Auton. Nerv. Syst. 76, 118–126.

Kim, Y.C., Gallo-Rodriguez, C., Jang, S.Y., Nandanan, E., Adams, M., Harden, T.K., Boyer, J.L., Jacobson, K.A., 2000. Acyclic analogues of deoxyadenosine 3′,5′-bisphosphates as $P2Y_1$ receptor antagonists. J. Med. Chem. 43, 746–755.

Klapperstuck, M., Buttner, C., Nickel, P., Schmalzing, G., Lambrecht, G., Markwardt, F., 2000. Antagonism by the suramin analogue NF279 on human $P2X_1$ and $P2X_7$ receptors. Eur. J. Pharmacol. 387, 245–252.

Krstew, E., Jarrott, B., Lawrence, A.J., 1998. Autoradiographic visualisation of axonal transport of adenosine A1 receptors along the rat vagus nerve and characterisation of adenosine A_1 receptor binding in the dorsal vagal complex of hypertensive and normotensive rats. Brain Res. 802, 61–68.

Lambrecht, G., 1996. Design and pharmacology of selective P2-purinoceptor antagonists. J. Auton. Pharmacol. 16, 341–344.

Lawrence, A.J., Castillo-Melendez, M., McLean, K.J., Jarrott, B., 1998. The distribution of nitric oxide synthase-, adenosine deaminase- and neuropeptide Y-immunoreactivity through the entire rat nucleus tractus solitarius: Effect of unilateral nodose ganglionectomy. J. Chem. Neuroanat. 15, 27–40.

Lawrence, A.J., Jarrott, B., 1996. Neurochemical modulation of cardiovascular control in the nucleus tractus solitarius. Prog. Neurobiol. 48, 21–53.

Lawrence, A.J., Watkins, D., Jarrott, B., 1995. Visualization of β-adrenoceptor binding sites on human inferior vagal ganglia and their axonal transport along the rat vagus nerve. J. Hypertens. 13, 631–635.

Lumme, A., Vanhatalo, S., Soinila, S., 1996. Axonal transport of nitric oxide synthase in autonomic nerves. J. Auton. Nerv. Syst. 56, 207–214.

Mateo, J., Garcia-Lecea, M., Miras-Portugal, M.T., Castro, E., 1998. Ca2+ signals mediated by P2X-type purinoceptors in cultured cerebellar Purkinje cells. J. Neurosci. 18, 1704–1712.

Megson, A.C., Dickenson, J.M., Townsend-Nicholson, A., Hill, S.J., 1995. Synergy between the inositol phosphate responses to transfected human adenosine A_1-receptors and constitutive P_2-purinoceptors in CHO-K1 cells. Br. J. Pharmacol. 115, 1415–1424.

Meldrum, L.A., Burnstock, G., 1985. Evidence that ATP is involved as a co-transmitter in the hypogastric nerve supplying the seminal vesicle of the guinea-pig. Eur. J. Pharmacol. 110, 363–366.

Moore, D., Chambers, J., Waldvogel, H., Faull, R., Emson, P., 2000. Regional and cellular distribution of the $P2Y_1$ purinergic receptor in the human brain: striking neuronal localisation. J. Comp. Neurol. 421, 374–384.

Moore, D.J., Chambers, J.K., Wahlin, J.P., Kong, K.B., Moore, G.B., Jenkins, O., Emson, P.C., Murdock, P.R., 2001. Expression pattern of human P2Y receptor subtypes: a quantitative reverse transcription-polymerase chain reaction study. Biochim. Biophys. Acta 1521, 107–119.

Moran-Jimenez, M.J., Matute, C., 2000. Immunohistochemical localization of the $P2Y_1$ purinergic receptor in neurons and glial cells of the central nervous system. Mol. Brain Res. 78, 50–58.
Nieber, K., Poelchen, W., Illes, P., 1997. Role of ATP in fast excitatory synaptic potentials in locus coeruleus neurones of the rat. Br. J. Pharmacol. 122, 423–430.
Paxinos, G., Watson, C., 1986. The Rat Brain in Stereotaxic Coordinates. Academic Press, Australia.
Poelchen, W., Sieler, D., Illes, P., 1999. Evidence for co-release of norepinephrine and ATP from nerve terminals of rat locus coeruleus neurons. Soc. Neurosci. Abstr. 25, 481411.
Pubill, D., Dayanithi, G., Siatka, C., Andres, M., Dufour, M.N., Giuillon, G., Mendre, C., 2001. ATP induces intracellular calcium increases and actin cytoskeleton disaggregation via P2x receptors. Cell Calcium 29, 299–309.
Ralevic, V., Burnstock, G., 1998. Receptors for purines and pyrimidines. Pharamcol. Rev. 50, 413–492.
Ralevic, V., Thomas, T., Burnstock, G., Spyer, K.M., 1999. Characterization of P2 receptors modulating neural activity in rat rostral ventrolateral medulla. Neuroscience 94, 867–878.
Rettinger, J., Schmalzing, G., Damer, S., Muller, G., Nickel, P., Lambrecht, G., 2000. The suramin analogue NF279 is a novel and potent antagonist selective for the $P2X_1$ receptor. Neuropharmacology 39, 2044–2053.
Rivkees, S.A., Price, S.L., Zhou, F.C., 1995. Immunohistochemical detection of A1 adenosine receptors in rat brain with emphasis on localization in the hippocampal formation, cerebral cortex, cerebellum and basal ganglia. Brain Res. 677, 193–203.
Schachter, J.B., Harden, T.K., 1997. An examination of deoxyadenosine 5′(alpha-thio)triphosphate as a ligand to define P2Y receptors and its selectivity as a low potency partial agonist of the $P2Y_1$ receptor. Br. J. Pharmacol. 121, 338–344.
Scislo, T.J., Ergene, E., Oleary, D.S., 1998. Impaired arterial baroreflex regulation of heart rate after blockade of P-2-purinoceptors in the nucleus tractus solitarius. Brain Res. Bull. 47, 63–67.
Scislo, T.J., O'Leary, D.S., 2000. Differential role of ionotropic glutamatergic mechanisms in responses to NTS P_{2x} and A_{2a} receptor stimulation. Am. J. Physiol. 278, H2057–H2068.
Shen, K.Z., North, R.A., 1993. Excitation of rat locus coeruleus neurons by adenosine 5′-triphosphate: ionic mechanism and receptor characterization. J. Neurosci. 13, 894–899.
Simon, J., Webb, T.E., Barnard, E.A., 1997. Distribution of [^{35}S]dATPαS binding sites in the adult rat neuraxis. Neuropharmacology 36, 1243–1251.
St Lambert, J.H., Dashwood, M.R., Spyer, K.M., 1996. Role of brainstem adenosine A_1 receptors in the cardiovascular response to hypothalamic defence area stimulation in the anaesthetized rat. Br. J. Pharmacol. 117, 227–282.
Strobaek, D., Olesen, S.P., Christophersen, P., Dissing, S., 1996. P2-purinoceptor-mediated formation of inositol phosphates and intracellular Ca2+ transients in human coronary artery smooth muscle cells. Br. J. Pharmacol. 118, 1645–1652.
Sun, M.K., Wahlestedt, C., Reis, D.J., 1992. Action of externally applied ATP on rat reticulospinal vasomotor neurons. Eur. J. Pharmacol. 224, 93–96.
Thomas, T., Spyer, K.M., 2000. ATP as a mediator of mammalian central CO_2 chemoreception. J. Physiol. 523, 441–447.
Vigne, P., Breittmayer, J.P., Frelin, C., 2000. Diadenosine polyphosphates as antagonists of the endogenous $P2Y_1$ receptor in rat brain capillary endothelial cells of the B7 and B10 clones. Br. J. Pharmacol. 129, 1506–1512.
Vigne, P., Hechler, B., Gachet, C., Breittmayer, J.P., Frelin, C., 1999. Benzoyl ATP is an antagonist of rat and human $P2Y_1$ receptors and of platelet aggregation. Biochem. Biophys. Res. Commun. 256, 94–97.
Virginio, C., North, R.A., Surprenant, A., 1998. Calcium permeability and block at homomeric and heteromeric $P2X_2$ and $P2X_3$ receptors, and P2X receptors in rat nodose neurones. J. Physiol. London 510, 27–35.
von Kügelgen, I., Wetter, A., 2000. Molecular pharmacology of P2Y-receptors. Naunyn-Schmiedeberg's Arch. Pharmacol. 362, 310–323.
Vulchanova, L., Arvidsson, U., Riedl, M., Wang, J., Buell, G., Surprenant, A., North, R.A., Elde, R., 1996. Differential distribution of two ATP-gated ion channels (P-2X receptors) determined by immunocytochemistry. Proc. Natl. Acad. Sci. USA 93, 8063–8067.
Vulchanova, L., Riedl, M.S., Shuster, S.J., Buell, G., Surprenant, A., North, R.A., Elde, R., 1997. Immunohistochemical study of the $P2X_2$ and $P2X_3$ receptor subunits in rat and monkey sensory neurons and their central terminals. Neuropharmacology 36, 1229–1242.
Webb, T.E., Feolde, E., Vigne, P., Neary, J.T., Runberg, A., Frelin, C., Barnard, E.A., 1996. The P2Y purinoceptor in rat brain microvascular endothelial cells couple to inhibition of adenylate cyclase. Br. J. Pharmacol. 119, 1385–1392.
Webb, T.E., Simon, J., Barnard, E.A., 1998. Regional distribution of [^{35}S]2′-deoxy 5′-O-(1-thio) ATP binding sites and the $P2Y_1$ messenger RNA within the chick brain. Neuroscience 84, 825–837.
Xiang, Z.H., Bo, X.N., Burnstock, G., 1998. Localization of ATP-gated P2X receptor immunoreactivity in rat sensory and sympathetic ganglia. Neurosci. Lett. 256, 105–108.
Yao, S.T., Barden, J.A., Finkelstein, D.I., Bennett, M.R., Lawrence, A.J., 2000. Comparative study on the distribution patterns of $P2X_1$-$P2X_6$ receptor immunoreactivity in the brainstem of the rat and the common marmoset (Callithrix jacchus): association with catecholamine cell groups. J. Comp. Neurol. 427, 485–507.
Yoshioka, K., Saitoh, O., Nakata, H., 2001. Heteromeric association creates a P2Y-like adenosine receptor. Proc. Natl. Acad. Sci. USA 98, 7617–7622.
Zambon, A.C., Brunton, L.L., Barrett, K.E., Hughes, R.J., Torres, B., Insel, P.A., 2001. Cloning, expression, signaling mechanisms, and membrane targeting of $P2Y_{11}$ receptors in Madin Darby canine kidney cells. Mol. Pharmacol. 60, 26–35.
Zhang, F.L., Luo, L., Gustafson, E., Lachowicz, J., Smith, M., Qiao, X., Liu, Y.H., Chen, G., Pramanik, B., Laz, T.M., Palmer, K., Bayne, M., Monsma, F.J., 2001. ADP is the cognate ligand for the orphan G protein-coupled receptor SP1999. J. Biol. Chem. 276, 8608–8615.
Zundorf, G., Schafer, R., Vohringer, C., Halbfinger, E., Fischer, B., Reiser, G., 2001. Novel modified adenosine 5′-triphosphate analogues pharmacologically characterized in human embryonic kidney 293 cells highly expressing rat brain $P2Y_1$ receptor: Biotinylated analogue potentially suitable for specific $P2Y_1$ receptor isolation. Biochem. Pharmacol. 61, 1259–1269.

(*Accepted* 15 *April* 2002)